Lead-free Cesium Europium Halide Perovskite Nanocrystals

Jianmei Huang[1,2,‡], Teng Lei[1,2,‡], Martin Siron[3], Ye Zhang[1,4], Sunmoon Yu[3,4], Fabian Seeler[5], Ahmad Dehestani[2,5], Li Na Quan[1,4], Kerstin Schierle-Arndt[2,5], and Peidong Yang[1,2,3,4,6,*]

[1] Department of Chemistry, University of California, Berkeley, California 94720, United States

[2] California Research Alliance (CARA) by BASF, Berkeley, California 94720, United States

[3] Department of Materials Science and Engineering, University of California, Berkeley, California 94720, United States

[4] Materials Sciences Division, Lawrence Berkeley National Laboratory, Berkeley, California 94720, United States

[5] BASF SE, Ludwigshafen am Rhein 67056, Germany

[6] Kavli Energy NanoScience Institute, Berkeley, California 94720, United States

ABSTRACT: Due to the toxicity of lead, searching for a lead-free halide perovskite semiconducting material with comparable optical and electronic properties is of great interest. Rare-earth based halide perovskite represents a promising class of materials for this purpose. In this work, we demonstrate the solution phase synthesis of single-crystalline $CsEuCl_3$ nanocrystals with a uniform size distribution centered around 15 nm. The $CsEuCl_3$ nanocrystals have photoluminescence emission centered at 435 nm, with a full width at half maximum (FWHM) of 19 nm. Furthermore, $CsEuCl_3$ nanocrystals can be embedded in a polymer matrix which provides enhanced stability under continuous laser irradiation. Lead-free rare earth cesium europium halide perovskite nanocrystals represent a promising candidate to replace lead halide perovskites.

KEYWORDS: rare earth; nanocrystals; blue emission; lead-free halide perovskites

Lead-based halide perovskites $APbX_3$ (A= CH_3NH_3, $CH(NH_2)_2$; X = Cl, Br, I) have emerged as a promising class of semiconducting materials for optoelectronic applications because of their long carrier diffusion length, high absorption coefficient, and bright photoluminescence property, especially the wide band-gap tunability and high defect tolerance.[1-4] Lead halide perovskites are comparable in optoelectronic performance to conventional semiconductor technology, yet, they can be synthesized via solution-based methods, making their fabrication versatile and low-cost. However, the toxicity of lead and the poor stability against moisture/heat in metal halide perovskites are two main challenges that need to be addressed.[5] Recently, the stability of the lead halide perovskite has been improved by replacing the organic A site cation with an inorganic cation such as Cs^+ or Rb^+, leading to an all inorganic halide perovskite.[6]

Compared to the bulk counterpart, halide perovskite nanocrystals have shown improved optical properties due to larger exciton binding energy, stronger excitonic absorption, and thus, higher photoluminescence quantum yield at room temperature.[7] Many efforts have been devoted to synthesizing different lead halide perovskite nanostructures.[8-11] However, the toxicity of lead is still an on-going concern for various applications such as photovoltaics and color-tunable light emitting diodes (LEDs).

To develop the lead-free halide perovskites with comparable optoelectronic performance is desired. Tin (Sn), with a similar valence configuration and ionic radius, was the first candidate to replace Pb.[12] However, the tin-based halide perovskites degrade fast in ambient air due to the ease of oxidation of tin from Sn^{2+} into Sn^{4+}.[13, 14] Direct synthesis of Sn^{4+} halide perovskites nanocrystals also present poor performance.[15] Double perovskite ($A_2M^+M^{3+}X_6$) and layer perovskite ($A_3M^{3+}{}_2X_9$) are another two types of lead-free halide perovskites. However, the double perovskite Cs_2AgBiX_6 (X=Cl, Br) nanocrystals presented weak photoluminescence due to their indirect band gap nature.[16, 17] In addition, lead free $Cs_3Bi_2Br_9$ and $Cs_3Sb_2Br_9$ perovskite nanocrystals exhibited strong photoluminescence (4.5%-46% quantum efficiency) while with broad full width at half maximum (FWHM) of 40-50 nm.[18-20] Therefore, lead-free perovskites with strong photoluminescence and narrow FWHM are needed to develop for better optoelectronic applications, such as high resolution and vivid display.

Rare earth halide perovskites, for example europium halide perovskite and ytterbium halide perovskite, are considered as promising lead-free perovskite candidates due to their luminescence properties reported previously.[21-23] The hybrid europium halide perovskite $(C_4H_9NH_3)_2EuI_4$ bulk crystal and the all inorganic $CsEuBr_3$ bulk crystal have shown strong blue emission with narrow FWHM of 25-35 nm, indicating that europium halide perovskites are potentially exciting new

materials for light emission.[21, 22] However, the europium halide perovskites bulk crystals synthesized via solid-state methods have limitations in controlling their uniformity and morphology. Colloidal synthesis of rare earth halide perovskite could potentially provide improved uniformity and tunable morphology. Lately, there are studies on the synthesis of Eu^{2+} doped CsBr nanocrystals and $CsEuBr_3$ nanocrystals, however, pure phase cesium europium halide perovskite still challenges. [24, 25]The low solubility of the rare earth precursors and potential oxidation of low-valence rare earth ions make such a method challenging.

In this work, we demonstrate the solution phase synthesis of cesium europium halide perovskite nanocrystals and have studied their unique optical properties. Furthermore, we embedded these $CsEuCl_3$ nanocrystals in a poly(methyl methacrylate) matrix and tested their stability under continuous laser irradiation. This work offers a promising alternative to lead-based halide perovskites including promising optical performance, enhanced stability and decreased toxicity.

Before we synthesized the $CsEuX_3$ nanocrystals, we found that the required precursors such as $EuCl_2$, are difficult to dissolve in non-polar solvents. Adding the traditional surfactant ligands such as oleic acid (OlAc), oleylamine (OlAm), and trioctylphosphine (TOP), used in lead-halide perovskite synthesis, negligibly increases the solubility of the rare earth precursors. Moreover, Eu^{2+} can be oxidized into Eu^{3+} with direct exposure to air. Eu^{2+} also has a strong tendency to bind with solvent molecules present,[26] impeding the formation of perovskite.

To overcome these issues, we used $EuCl_3$ as an initial precursor and firstly reduced Eu^{3+} to Eu^{2+} using oleylamine as a reagent. This reducing protocol was demonstrated by previous study of synthesis of EuSe and EuS nanocrystals[27, 28] Cesium oleate was then injected into a non-

coordinating solvent, such as octadecene, along with the first-step obtained Eu^{2+} precursor in the presence of OlAc and TOP at 250 °C (**Fig. 1a**). After 45 min the reaction was quenched using an ice-water bath. The obtained solution was transferred to an Argon glovebox. More experimental details can be found in the supplementary information (SI). The crystal structure of these nanocrystals was confirmed by XRD. A sample of the as synthesized product was loaded into a capillary tube for measuring in-solution XRD. The resulting XRD matched well with the standard pattern of $CsEuCl_3$ (tetragonal, P4mm, PDF#01-084-0484, a=b=5.59 Å, c=5.62 Å) (**Fig. 1b, c**). It is difficult to distinguish the tetragonal and cubic (Pm-3m, PDF#01-075-1838, a=b=c=5.62 Å) phases due to the peak broadening of the small size of nanocrystals and the minor difference of XRD patterns of these two phases. The lattice constants of (100), (110) and (111) crystal planes are 5.59 Å, 3.95 Å and 3.23 Å, respectively, based on the tetragonal phase.

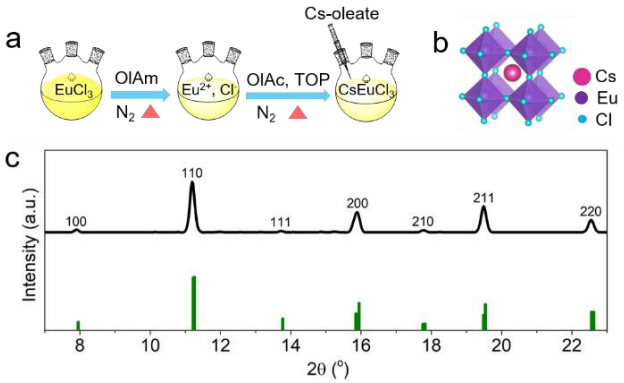

Figure 1 (a) Schematic of $CsEuCl_3$ nanocrystal synthesis. (b) Scheme of extended unit cell of $CsEuCl_3$. (c) XRD pattern of $CsEuCl_3$ nanocrystals (top) and standard XRD pattern of $CsEuCl_3$ (bottom). X-ray wavelength λ = 0.775 Å

Transmission Electron Microscopy (TEM) characterization was carried out to study the morphology, phase and composition of the nanocrystals. TEM image shows that the obtained nanocrystals are around 15 nm in diameter (**Fig. 2a**). Low magnification TEM images further confirm the homogeneous size distribution of the nanocrystals (**Fig. S1**). The phase of the nanocrystals was further characterized by Selected Area Electron Diffraction (SAED). Due to the weak signal from the individual single nanocrystal, we selected a large area with multiple nanocrystals and took the electron diffraction image. The diffraction pattern presents several rings rather than individual dots, resulting from the different orientations of nanocrystals. The clear diffraction rings from the (110), (200), (211) and (220) crystal planes of the $CsEuCl_3$ tetragonal phase were observed, which is consistent with the XRD result (**Fig. 2b**). From High Resolution TEM (HR-TEM) and the corresponding Fast Fourier Transform (FFT), it is clear that the nanocrystals are single-crystalline (**Fig. 2c and Fig. S2**). The FFT and XRD both confirm a lattice constant of 0.56 nm, consistent with the lattice spacing of (100) plane of $CsEuCl_3$. Energy Dispersive Spectroscopy (EDS) mapping demonstrates uniform distribution of Cs, Eu and Cl in the nanocrystals, and EDS quantification reveals a composition ratio of 18.4:20.2:61.4, close to the expected 1:1:3 perovskite ratio (**Fig. 2d, Fig. S3 and Table S1**).

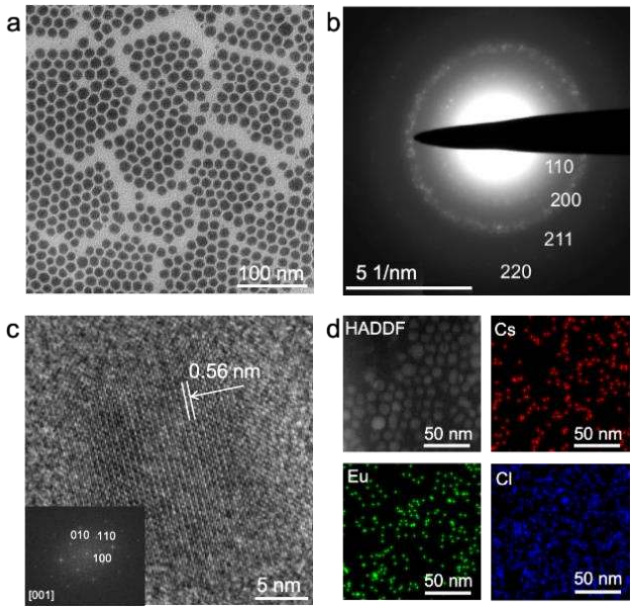

Figure 2 (a) Representative TEM image, (b) SAED pattern, (c) HRTEM and corresponding FFT (inset) and (d) EDS mapping of $CsEuCl_3$ nanocrystals.

The $CsEuCl_3$ nanocrystals show a strong excitonic absorption at around 350 nm. The optical band gap was estimated to be 3.09 eV from the absorption Tauc plot (**Fig. 3a**). The monodispersed colloidal nanocrystals show a blue emission centered at 435 nm with a narrow full width at half maximum (FWHM) of 19 nm (**Fig. 3b)**. Photoluminescence excitation (PLE) measurement was conducted at 435 nm emission wavelength and the spectrum is consistent with the absorption spectrum, which confirms the light emission is originated from the absorption of nanocrystals. The photoluminescence quantum yield (PLQY) of colloidal nanocrystals was calculated to be 2%±0.3% at room temperature. To determine the photogenerated carrier's lifetime of $CsEuCl_3$ nanocrystals, the time-resolved PL (TRPL) was conducted at the wavelength of 435 nm at room temperature. Referring to previous studies of lead-based and bismuth-based halide perovskite nanocrystals, TRPL decay curve usually gives the sum of non-radiative and radiative recombination rates.[8, 9, 29]

The TRPL decay curve of $CsEuCl_3$ nanocrystals was fitted to a biexponential decay function with a short-lived non-radiative component of 4.4 ns and a long-lived radiative component of 30.9 ns (**Fig. 3c**). Power dependent TRPL spectra was also measured at 435 nm for $CsEuCl_3$ nanocrystals. The lifetime increases as the power density of the laser increases, which may indicate that free carriers contribute to the emission (**Fig. S4**). The PL quenching and lifetime shortening by comparing PL and TRPL on only $CsEuCl_3$ nanocrystals thin film and introduction of an electron transporting layer (phenyl-C_{61}-butyric acid methyl ester, PCBM) on top of $CsEuCl_3$ nanocrystals thin film further suggest that the presence of free carriers contribution as the emission mechanisms, although we may not exclude the contribution from the $4f^6 5d^1$-$4f^7$ transition from Eu^{2+} (**Fig. S5 and Fig. S6**).

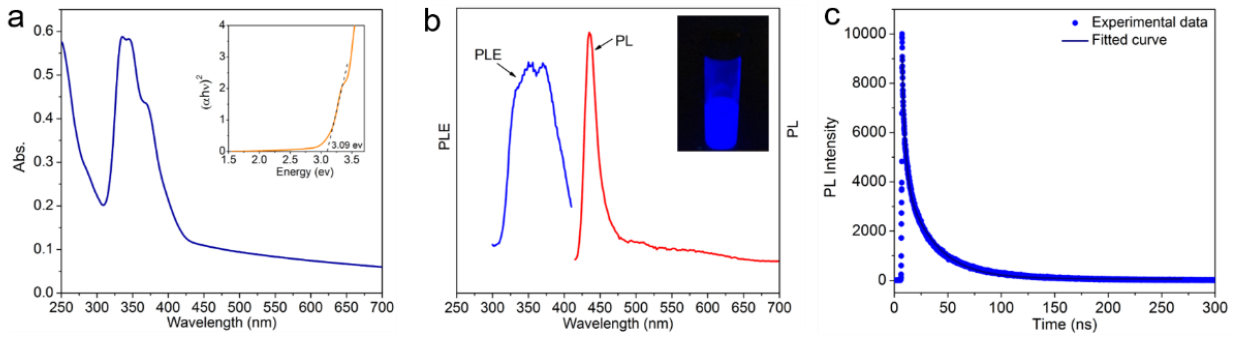

Figure 3 (a) Optical absorption and Tauc plot (inset) of absorption measurements of $CsEuCl_3$ nanocrystals. Assuming direct transition, we derive a band gap of 3.09 eV. (b) Photoluminescence (red) and photoluminescence excitation (blue) spectra collected at 435 nm. The inset picture shows the $CsEuCl_3$ nanocrystals under 365 nm UV lamp. (c) Time-resolved photoluminescence spectrum measures the decay of photoluminescence at 435 nm.

Surface treatment has been extensively applied to improve the PLQY in halide perovskite nanocrystals.[9, 30-32] 1-butyl-1-methylpyridinium chloride was used to synthesize lead-free antimony halide perovskite, which has strong photoluminescence.[33] Inspired by those studies, we applied 1-butyl-1-methylpyridinium chloride to passivate the $CsEuCl_3$ nanocrystals. The PLQY of $CsEuCl_3$ nanocrystals can be increased to 5.7%±0.3% and the PL peak position remain identical after surface treatment (**Fig. S7**). We compared TRPL measurements for as synthesized nanocrystals (~2.0% PLQY) and surface treated nanocrystals (~5.7% PLQY), it is clearly observed the PL kinetics of passivated nanocrystals is slower than the non-passivated nanocrystals (**Fig. S8)**. The surface chemistry and passivation of the semiconductor nanocrystals would have a great influence on their carrier lifetime; if the surface of nanocrystals well passivated, reduced surface defects will give rise to the increased carrier lifetimes. Likely, in our case, the ionic ligand acts as a chlorine source to substitute the chloride vacancy in the nanocrystal surface to reduce the surface defects, thereby increasing the PLQY (**Fig. S9**). This is further confirmed by ligand-concentration dependent PLQY measurements. As the ligand concentration increases from 0.01 μmol/mL to 1 μmol/mL, the PLQY also increases (**Fig. S10**). This could be due to an increase in surface passivation from chlorine ions. Ionic ligands with shorter carbon chain would be easier to release chlorine source to substitute chloride vacancy and have stronger interaction with $CsEuCl_3$ nanocrystals, which will be expected to further increase PLQY. Besides, according to the recent study on improving PLQY of $CsPbBr_3$ nanocrystals,[34] other ligands with "Cl-equivalent" effect, which play a role similar to chlorine ions and form strong interaction with europium ions, may also further improve the PLQY.

Rare earth ions can also act as a color center when doped into solid matrices, a topic which has been extensively investigated for optoelectronics, photonics, sensors and biomedical

applications.[35] Solid matrices doped with rare earth ions typically show large Stokes shift and long photoluminescence lifetime. Rare earths doping into solid matrices can be readily achieved via solid state or solution phase methods.[36, 37] To distinguish the non-perovskites structure of Eu^{2+} doped CsCl with the synthesized $CsEuCl_3$ perovskites, we successfully synthesized Eu^{2+} doped CsCl nanocrystals. These Eu^{2+} doped CsCl nanocrystals are around 50 nm in diameter (**Fig. S11a**). The doped CsCl structure is confirmed by XRD (**Fig. S11b**). HRTEM shows a lattice constant of 0.41 nm, which is consistent with the lattice spacing of the (100) plane of CsCl (**Fig. S11c**). The corresponding Fast Fourier Transform (FFT) from high-resolution TEM reveals the single-crystalline nature of the CsCl nanocrystals. Furthermore, EDS mapping clearly shows that Eu is homogeneously distributed in the nanocrystals, and EDS quantification indicates a doping level of around 1.3% (**Fig. S12, S13 and Table S2**). The doping percentage of Eu reported here is with respect to the total number of atoms, i.e. Cs, Eu and Cl.

Unlike $CsEuCl_3$ perovskite, Eu^{2+} doped CsCl nanocrystals show PL emission centered at 445 nm with a FWHM of 30 nm (**Fig. S14a**). This emission originates from the $4f^6 5d^1$-$4f^7$ transition of Eu^{2+} instead of the band edge,[38] leading to a larger FWHM when compared to the emission of $CsEuCl_3$. Eu^{2+} doped CsCl nanocrystals show a longer PL lifetime of 178 ns compared to the lifetime of $CsEuCl_3$ nanocrystals (**Fig. S14b**). This is consistent with previous research of Eu^{2+} doped halide or oxide matrices which have long PL lifetime in the range of hundreds of nanoseconds to a few microseconds[38, 39], while the short lifetime of $CsEuCl_3$ nanocrystals may indicate that the free carriers could contribute to the emission. Power-dependent TRPL was measured at 445 nm for Eu^{2+} doped CsCl nanocrystals. The PL decay curve shows negligible dependence on the excitation laser power density, affirming the origin of PL emission from an

orbital transition within the europium instead of photogenerated free carriers. This is very different from $CsEuCl_3$ nanocrystals, and it suggests different emission mechanism. (**Fig. S15**).

The $CsEuCl_3$ nanocrystals in toluene are stable for several months in inert atmosphere. However, when we drop-casted nanocrystals on a glass substrate and exposed them to air for several hours, additional red emissions from orbital transition of the Eu^{3+} (peaks at 593 nm, 615 nm, 650 nm and 698 nm, **Fig. S16**) would be observed due to the decomposition/oxidization of nanocrystals caused by moisture/oxygen. To protect the as-synthesized $CsEuCl_3$ nanocrystals from oxygen and moisture in the air, the nanocrystals were embedded into a PMMA polymer matrix. The PMMA matrix causes lower contrast in the TEM images due to lack of diffraction (**Fig. S17**), however it offers important protection to the nanocrystals against moisture and oxygen. The encapsulated nanocrystals show a blue emission centered at 436 nm with a FWHM of 35 nm. The distribution of nanoparticle size would affect the FWHM of PL spectrum.[40] The PL spectra became broader after embedding $CsEuCl_3$ nanocrystals into PMMA likely due to the aggregation of nanocrystals in PMMA matrix during the solvent evaporation process on the glass substrate. The shoulder in PL spectrum become greatly weaken in comparison with the unencapsulated nanocrystals may result from the passivation of PMMA. Previous study reported that PMMA could passivate the defects caused by the dangling bonds localized at the perovskite surface.[41, 42] The encapsulated nanocrystals show long optical stability under continuous laser irradiation with a power density of $4 W/cm^2$. The PL peak position and intensity changed negligibly during 380-min of irradiation measurements on the encapsulated nanocrystals (**Fig. 4**). Furthermore, there was no emission detected from the Eu^{3+} transitions. PMMA can thus effectively protect the nanocrystals.

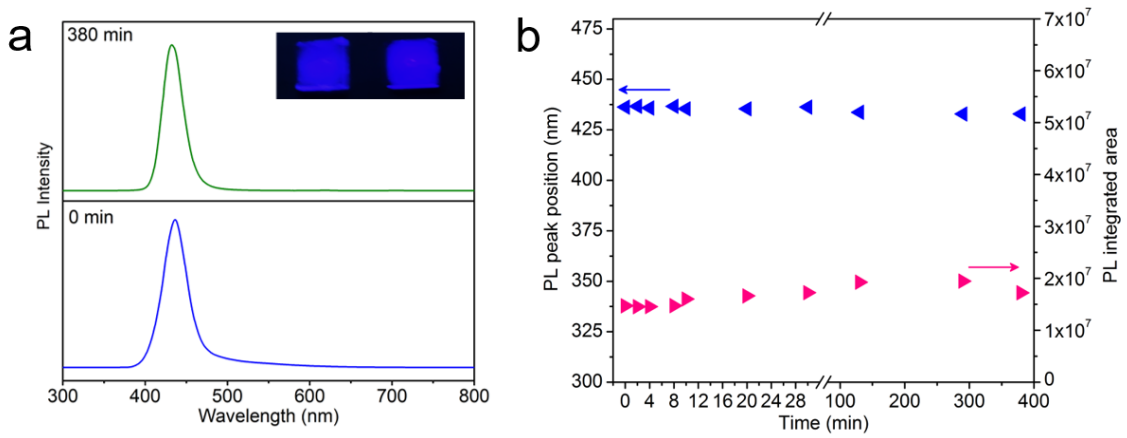

Figure 4 (a) Photoluminescence spectra of measurement before and after 380-min of continuous irradiation by laser on $CsEuCl_3$ nanocrystals embedded in PMMA. The inset picture shows the $CsEuCl_3$ nanocrystals-PMMA thin films under 365 nm UV lamp. (b) Emission peak position and integrated intensity during 380-min of continuous irradiation by laser.

In summary, a colloidal solution phase synthetic approach has been developed to obtain single-crystalline $CsEuCl_3$ nanocrystals with uniform size distribution centered around 15 nm. Optical studies determined that the $CsEuCl_3$ nanocrystals exhibit a sharp emission peak at 435 nm with narrow FWHM of 19 nm, which is one of unique property in lead-free perovskite in comparison with other reported lead-free perovskites with broad emission FWHM. Such narrow emission can improve the color purity and saturation, and increase the resolution of imaging, which is conductive to generate a more vivid and sharper image in display applications. Furthermore, these $CsEuCl_3$ nanocrystals embedded in a polymer matrix are stable under continuous irradiation by laser, presenting good stability towards moisture, oxygen and radiation. Such good stability makes them more promising to the practical application. This work illustrates that $CsEuCl_3$

nanocrystals are a promising candidate to replace lead halide perovskites. The synthetic methods reported here can potentially be applied to other rare earth halide perovskites.

ASSOCIATED CONTENT

Supporting Information. The Supporting Information of more experimental detail, characterizations and optical measurement (PDF) is available free of charge on the ACS Publications website at DOI: xxx.

AUTHOR INFORMATION

Corresponding Author

* E-mail: p_yang@berkeley.edu

Present Addresses

†Present address of Jianmei Huang: School of Energy and Power Engineering, Beihang University, Beijing, China.

Author Contributions

The manuscript was written through contributions of all authors. All authors have given approval to the final version of the manuscript. ‡ J.H. and T.L. contributed equally.

Notes

The authors declare no competing financial interests.

ACKNOWLEDGMENT

This work was financially supported by the BASF CARA program (No. 241053). Work at the NCEM, the Molecular Foundry and the Advanced Light Source was supported by the Office of Science, Office of Basic Energy Sciences of the U.S. Department of Energy under Contract No. DE-AC02-05CH11231. We thank Jia Lin and Hong Chen for valuable discussion, and also acknowledge Sheena Louisia and Sirine Fakra for assistance with XRD measurement at the Beamline 10.3.2 at the Advanced Light Source. T. L., and Y. Z. acknowledge the fellowship support from Suzhou Industrial Park. M. S. acknowledges support from the National Science Foundation Graduate Research Fellowship under Grant No. DGE 1752814. S.Y. acknowledges support from Samsung Scholarship.

REFERENCES

1. Green, M. A.; Ho-Baillie, A.; Snaith, H. J. The emergence of perovskite solar cells. *Nat. Photonics* **2014,** 8, 506-514.

2. Manser, J. S.; Christians, J. A.; Kamat, P. V. Intriguing Optoelectronic Properties of Metal Halide Perovskites. *Chem. Rev.* **2016,** 116, (21), 12956-13008.

3. Stranks, S. D.; Snaith, H. J. Metal-halide perovskites for photovoltaic and light-emitting devices. *Nat. Nanotech.* **2015,** 10, 391-402.

4. Lei, T.; Lai, M.; Kong, Q.; Lu, D.; Lee, W.; Dou, L.; Wu, V.; Yu, Y.; Yang, P. Electrical and Optical Tunability in All-Inorganic Halide Perovskite Alloy Nanowires. *Nano Lett.* **2018,** 18, (6), 3538-3542.

5. Giustino, F.; Snaith, H. J. Toward Lead-Free Perovskite Solar Cells. *ACS Energy Lett.* **2016,** 1, (6), 1233-1240.

6. Service, R. F. Cesium fortifies next-generation solar cells. *Science* **2016,** 351, (6269), 113-114.

7. Huang, J.; Lai, M.; Lin, J.; Yang, P. Rich Chemistry in Inorganic Halide Perovskite Nanostructures. *Adv. Mater.* 2018, 1802856.

8. Protesescu, L.; Yakunin, S.; Bodnarchuk, M. I.; Krieg, F.; Caputo, R.; Hendon, C. H.; Yang, R. X.; Walsh, A.; Kovalenko, M. V. Nanocrystals of Cesium Lead Halide Perovskites (CsPbX3, X = Cl, Br, and I): Novel Optoelectronic Materials Showing Bright Emission with Wide Color Gamut. *Nano Lett.* **2015,** 15, (6), 3692-3696.

9. Zhang, D.; Yang, Y.; Bekenstein, Y.; Yu, Y.; Gibson, N. A.; Wong, A. B.; Eaton, S. W.; Kornienko, N.; Kong, Q.; Lai, M.; Alivisatos, A. P.; Leone, S. R.; Yang, P. Synthesis of Composition Tunable and Highly Luminescent Cesium Lead Halide Nanowires through Anion-Exchange Reactions. *J. Am. Chem. Soc.* **2016,** 138, (23), 7236-7239.

10. Bekenstein, Y.; Koscher, B. A.; Eaton, S. W.; Yang, P.; Alivisatos, A. P. Highly luminescent colloidal nanoplates of perovskite cesium lead halide and their oriented assemblies. *J. Am. Chem. Soc* **2015,** 137, (51), 16008-16011.

11. Shamsi, J.; Dang, Z.; Bianchini, P.; Canale, C.; Di Stasio, F.; Brescia, R.; Prato, M.; Manna, L. Colloidal synthesis of quantum confined single crystal CsPbBr3 nanosheets with lateral size control up to the micrometer range. *J. Am. Chem. Soc.* **2016,** 138, (23), 7240-7243.

12. van der Stam, W.; Geuchies, J. J.; Altantzis, T.; van den Bos, K. H. W.; Meeldijk, J. D.; Van Aert, S.; Bals, S.; Vanmaekelbergh, D.; de Mello Donega, C. Highly Emissive Divalent-Ion-Doped Colloidal CsPb1–xMxBr3 Perovskite Nanocrystals through Cation Exchange. *J. Am. Chem. Soc.* **2017,** 139, (11), 4087-4097.

13. Jellicoe, T. C.; Richter, J. M.; Glass, H. F. J.; Tabachnyk, M.; Brady, R.; Dutton, S. E.; Rao, A.; Friend, R. H.; Credgington, D.; Greenham, N. C.; Böhm, M. L. Synthesis and Optical Properties of Lead-Free Cesium Tin Halide Perovskite Nanocrystals. *J. Am. Chem. Soc.* **2016,** 138, (9), 2941-2944.

14. Wong, A. B.; Bekenstein, Y.; Kang, J.; Kley, C. S.; Kim, D.; Gibson, N. A.; Zhang, D.; Yu, Y.; Leone, S. R.; Wang, L.-W.; Alivisatos, A. P.; Yang, P. Strongly Quantum Confined Colloidal Cesium Tin Iodide Perovskite Nanoplates: Lessons for Reducing Defect Density and Improving Stability. *Nano Lett.* **2018,** 18, (3), 2060-2066.

15. Wang, A.; Yan, X.; Zhang, M.; Sun, S.; Yang, M.; Shen, W.; Pan, X.; Wang, P.; Deng, Z. Controlled synthesis of lead-free and stable perovskite derivative Cs2SnI6 nanocrystals via a facile hot-injection process. *Chem. Mater.* **2016,** 28, (22), 8132-8140.

16. Bekenstein, Y.; Dahl, J. C.; Huang, J.; Osowiecki, W. T.; Swabeck, J. K.; Chan, E. M.; Yang, P.; Alivisatos, A. P. The Making and Breaking of Lead-Free Double Perovskite

Nanocrystals of Cesium Silver–Bismuth Halide Compositions. *Nano Lett.* **2018,** 18, (6), 3502-3508.

17. Creutz, S. E.; Crites, E. N.; De Siena, M. C.; Gamelin, D. R. Colloidal Nanocrystals of Lead-Free Double-Perovskite (Elpasolite) Semiconductors: Synthesis and Anion Exchange To Access New Materials. *Nano Lett.* **2018,** 18, (2), 1118-1123.

18. Leng, M.; Yang, Y.; Zeng, K.; Chen, Z.; Tan, Z.; Li, S.; Li, J.; Xu, B.; Li, D.; Hautzinger, M. P.; Fu, Y.; Zhai, T.; Xu, L.; Niu, G.; Jin, S.; Tang, J. All-Inorganic Bismuth-Based Perovskite Quantum Dots with Bright Blue Photoluminescence and Excellent Stability. *Adv. Funct. Mater.* **2018,** 28, (1), 1704446.

19. Zhang, J.; Yang, Y.; Deng, H.; Farooq, U.; Yang, X.; Khan, J.; Tang, J.; Song, H. High Quantum Yield Blue Emission from Lead-Free Inorganic Antimony Halide Perovskite Colloidal Quantum Dots. *ACS Nano* **2017,** 11, (9), 9294-9302.

20. Yang, B.; Chen, J.; Hong, F.; Mao, X.; Zheng, K.; Yang, S.; Li, Y.; Pullerits, T.; Deng, W.; Han, K. Lead-Free, Air-Stable All-Inorganic Cesium Bismuth Halide Perovskite Nanocrystals. *Angew. Chem. Int. Ed.* **2017,** 56, (41), 12471-12475.

21. Mitzi, D. B.; Liang, K. Preparation and Properties of (C4H9NH3)2EuI4: A Luminescent Organic−Inorganic Perovskite with a Divalent Rare-Earth Metal Halide Framework. *Chem. Mater.* **1997,** 9, (12), 2990-2995.

22. Hesse, S.; Zimmermann, J.; von Seggern, H.; Ehrenberg, H.; Fuess, H.; Fasel, C.; Riedel, R. CsEuBr3: Crystal structure and its role in the photostimulation of CsBr:Eu2+. *J. Appl. Phys.* **2006,** 100, (8), 083506.

23. Moon, B. J.; Kim, S. J.; Lee, S.; Lee, A.; Lee, H.; Lee, D. S.; Kim, T.-W.; Lee, S.-K.; Bae, S.; Lee, S. H. Rare-Earth-Element-Ytterbium-Substituted Lead-Free Inorganic Perovskite Nanocrystals for Optoelectronic Applications. *Adv. Mater.* **2019,** 31, (33), 1901716.

24. Yang, Z. W.; Jiang, Z.; Liu, X. Y.; Zhou, X. C.; Zhang, J. H.; Li, W. W. Bright Blue Light-Emitting Doped Cesium Bromide Nanocrystals: Alternatives of Lead-Free Perovskite Nanocrystals for White LEDs. *Adv. Opt. Mater.* **2019,** 7, (10), 1900108.

25. Alam, F.; Wegner, K. D.; Pouget, S.; Amidani, L.; Kvashnina, K.; Aldakov, D.; Reiss, P. Eu2+: A suitable substituent for Pb2+ in CsPbX3 perovskite nanocrystals? *J. Chem. Phys.* **2019,** 151, (23), 231101- 231107.

26. Garcia, J.; Allen, M. J. Developments in the Coordination Chemistry of Europium(II). *Eur. J. Inorg. Chem.* **2012,** 2012, (29), 4550-4563.

27. Wang, C.; Zhang, D.; Xu, L.; Jiang, Y.; Dong, F.; Yang, B.; Yu, K.; Lin, Q. A Simple Reducing Approach Using Amine To Give Dual Functional EuSe Nanocrystals and Morphological Tuning. *Angew. Chem.* **2011,** 123, (33), 7729-7733.

28. Zhao, F.; Sun, H.-L.; Su, G.; Gao, S. Synthesis and Size-Dependent Magnetic Properties of Monodisperse EuS Nanocrystals. *Small* **2006,** 2, (2), 244-248.

29. Slavney, A. H.; Hu, T.; Lindenberg, A. M.; Karunadasa, H. I. A Bismuth-Halide Double Perovskite with Long Carrier Recombination Lifetime for Photovoltaic Applications. *J. Am. Chem. Soc.* **2016,** 138, (7), 2138-2141.

30. Almeida, G.; Infante, I.; Manna, L. Resurfacing halide perovskite nanocrystals. *Science* **2019,** 364, (6443), 833-834.

31. Koscher, B. A.; Swabeck, J. K.; Bronstein, N. D.; Alivisatos, A. P. Essentially Trap-Free CsPbBr3 Colloidal Nanocrystals by Postsynthetic Thiocyanate Surface Treatment. *J. Am. Chem. Soc.* **2017,** 139, (19), 6566-6569.

32. Krieg, F.; Ochsenbein, S. T.; Yakunin, S.; ten Brinck, S.; Aellen, P.; Süess, A.; Clerc, B.; Guggisberg, D.; Nazarenko, O.; Shynkarenko, Y.; Kumar, S.; Shih, C.-J.; Infante, I.; Kovalenko, M. V. Colloidal CsPbX3 (X = Cl, Br, I) Nanocrystals 2.0: Zwitterionic Capping Ligands for Improved Durability and Stability. *ACS Energy Lett.* **2018,** 3, (3), 641-646.

33. Zhou, C.; Lin, H.; Tian, Y.; Yuan, Z.; Clark, R.; Chen, B.; van de Burgt, L. J.; Wang, J. C.; Zhou, Y.; Hanson, K.; Meisner, Q. J.; Neu, J.; Besara, T.; Siegrist, T.; Lambers, E.; Djurovich, P.; Ma, B. Luminescent zero-dimensional organic metal halide hybrids with near-unity quantum efficiency. *Chem. Sci.* **2018,** 9, (3), 586-593.

34. Yang, D.; Li, X.; Zhou, W.; Zhang, S.; Meng, C.; Wu, Y.; Wang, Y.; Zeng, H. CsPbBr3 Quantum Dots 2.0: Benzenesulfonic Acid Equivalent Ligand Awakens Complete Purification. *Adv. Mater.* **2019,** 31, (30), 1900767.

35. Bai, G.; Tsang, M.-K.; Hao, J. Luminescent Ions in Advanced Composite Materials for Multifunctional Applications. *Adv. Funct. Mater.* **2016,** 26, (35), 6330-6350.

36. Li, P.; Zhang, Y.; Zhang, L.; Li, F.; Guo, Y.; Li, Y.; Gao, W. Phase Control of Eu3+-Doped YPO4 Nano-/Microcrystals. *Cryst. Growth Des.* **2017,** 17, (11), 5935-5944.

37. Saeki, K.; Koshimizu, M.; Fujimoto, Y.; Yanagida, T.; Okada, G.; Yahaba, T.; Tanaka, H.; Asai, K. Scintillation properties of Eu-doped CsCl and CsBr crystals. *Opt. Mater.* **2016,** 61, 125-128.

38. Kobayasi, T.; Mroczkowski, S.; Owen, J. F.; Brixner, L. H. Fluorescence lifetime and quantum efficiency for 5d → 4f transitions in Eu2+ doped chloride and fluoride crystals. *J. Luminescence* **1980,** 21, (3), 247-257.

39. Zhang, S.; Huang, Y.; Seo, H., *Luminescence properties and structure of Eu2+ doped KMgPO4 phosphor*. *Opt. Mater.* **2010,** 32, 1545-1548.

40. Sun, J.; Yang, J.; Lee, J. I.; Cho, J. H.; Kang, M. S. Lead-Free Perovskite Nanocrystals for Light-Emitting Devices. *J. Phys. Chem. Lett.* **2018**, 1573-1583.

41. Peng, J.; Wu, Y.; Ye, W.; Jacobs, D. A.; Shen, H.; Fu, X.; Wan, Y.; Duong, T.; Wu, N.; Barugkin, C.; Nguyen, H. T.; Zhong, D.; Li, J.; Lu, T.; Liu, Y.; Lockrey, M. N.; Weber, K. J.; Catchpole, K. R.; White, T. P. Interface passivation using ultrathin polymer–fullerene films for high-efficiency perovskite solar cells with negligible hysteresis. *Energ. Environ. Sci.* **2017,** 10, (8), 1792-1800.

42. Kong, W.; Ding, T.; Bi, G.; Wu, H. Optical characterizations of the surface states in hybrid lead–halide perovskites. *Phys. Chem. Chem. Phys.* **2016,** 18, (18), 12626-12632.

Table of Contents

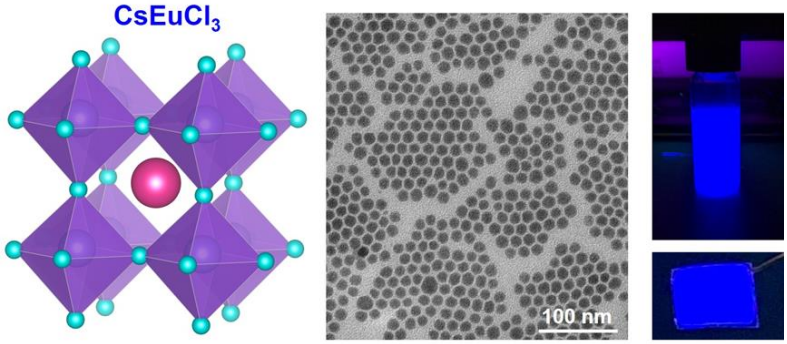

Supporting Information

Lead-free Cesium Europium Halide Perovskite Nanocrystals

Jianmei Huang[1,2,‡], Teng Lei[1,2,‡], Martin Siron[3], Ye Zhang[1,4], Sunmoon Yu[3,4], Fabian Seeler[5], Ahmad Dehestani[2,5], Li Na Quan[1,4], Kerstin Schierle-Arndt[2,5], and Peidong Yang[1,2,3,4,6,*]

[1] Department of Chemistry, University of California, Berkeley, California 94720, United States
[2] California Research Alliance (CARA) by BASF, Berkeley, California 94720, United States
[3] Department of Materials Science and Engineering, University of California, Berkeley, California 94720, United States
[4] Materials Sciences Division, Lawrence Berkeley National Laboratory, Berkeley, California 94720, United States
[5] BASF SE, Ludwigshafen am Rhein 67056, Germany
[6] Kavli Energy NanoScience Institute, Berkeley, California 94720, United States

Experimental details:

Chemicals:
Cs_2CO_3 (99.9%, Aldrich), $EuCl_3$ (99.99%, Alfa Aesar), 1-octadecene (ODE, 90%, Aldrich), oleic acid (OlAc, 90%, Aldrich), octanoic acid (OctAc, 99%, Aldrich), oleylamine (OlAm, Aldrich, 70%), trioctylphosphine (TOP, 97%, Aldrich), 1-butyl-1-methylpyridinium chloride (>98%, TCI), phenyl-C_{61}-butyric acid methyl ester (PCBM, Sigma-Aldrich), poly(methyl methacrylate) (PMMA, average M_w ~350,000, Sigma-Aldrich), hexane (anhydrous, 95%, Sigma-Aldrich), toluene (anhydrous, 99.8%, Sigma-Aldrich). All chemicals were used as received without further purification.

Preparation of Cs-oleate solution:
0.2 g Cs_2CO_3 and 0.7 mL OlAc were loaded into a 3-neck flask and dissolved in 7.5 mL ODE. The flask was degassed and dried under vacuum at 120 °C for 40 min, and then heated under N_2 to 150 °C until all Cs_2CO_3 reacted with OlAc.

Preparation of Eu^{2+} precursor:
1 mmol $EuCl_3$ and 5 mL OlAm were loaded into a 3-neck flask and degassed under vacuum for 60 mins at 120 °C. The temperature was then raised to 300 °C under N_2 and kept for 40 mins to reduce the europium precursor. The obtained Eu^{2+} precursor was cooled down to room temperature and then transferred to the glove box for further use.

Synthesis of $CsEuCl_3$ nanocrystals:
For a standard reaction, 5 mL ODE, 0.25 mL OlAc and 0.5 mL TOP were loaded into a 3-neck flask and degassed under vacuum for 60 mins at 120 °C. Then 2 mL of Eu^{2+} precursor was injected under N_2 and temperature was raised to 250 °C and kept for 25 mins. 1 mL of Cs-oleate solution was swiftly injected. After 45 minutes, the reaction was quenched by cooling the flask in an ice-water bath. 6 ml of hexane was added into the obtained crude solution and the nanocrystals were isolated by centrifugation at 8000 rpm for 5 mins and washed once with hexane. The obtained precipitated nanocrystals were re-dispersed in hexane or toluene and centrifuged at 4000 rpm for 1 min. The supernatant was kept while the aggregated nanocrystals were discarded.

Synthesis of Eu^{2+} doped CsCl nanocrystals:
For a standard reaction, 5 mL ODE and 1 mL OctAc were loaded into a 3-neck flask and degassed under vacuum for 60 mins at 120 °C. Then 1 mL of Eu^{2+} precursor was injected under N_2 and temperature was raised to 200 °C and kept for 15 mins. 0.5 mL of Cs-oleate solution was swiftly injected. After 5 minutes, the reaction was quenched by cooling the flask in an ice-water bath. The nanocrystals were isolated by centrifugation of the obtained crude solution at 8000 rpm for 5 mins and washed once with hexane or toluene. The obtained precipitated nanocrystals were re-dispersed in hexane or toluene.

Surface treatment:
Anhydrous toluene (5 mL), 1-butyl-1-methylpyridinium chloride (0.05 mmol), OlAc (0.5 mL) and OlAm (0.5 mL) were added to a scintillation vial within an argon inert atmosphere glovebox. The solution was stirred at 100 °C on a hot plate within the glovebox until the complete dissolution of the 1-butyl-1-methylpyridinium chloride. The resulting concentrated stock solution is stored in a glovebox to limit the water content of the solution over time. Then the stock solution was diluted to different concentration for further surface treatment. The cleaned $CsEuCl_3$ nanocrystals solution was then mixed with the above solution and was stirred at 100°C hot plate for 1.5 hours.

Preparation of $CsEuCl_3$ nanocrystals thin film, and PCBM thin film on top of $CsEuCl_3$ nanocrystals thin film:
The $CsEuCl_3$ nanocrystals was spin-coated on a glass substrate at 3000 rpm for 60s. Then a 10mg/mL PCBM solution in chloroform was spin-coated at 3000 rpm on top of the perovskite layer.

$CsEuCl_3$ nanocrystals embedded in matrix:
PMMA was well dissolved in toluene. Then, $CsEuCl_3$ nanocrystals solution was added into this PMMA solution. Sonication was applied to create a homogeneous solution. The obtained solution was spin-coated to achieve a transparent thin film.

Characterization:
Micro-X-ray diffraction (μXRD) data of $CsEuCl_3$ nanocrystals was collected using an incident X-ray energy of 16 keV (λ = 0.775 Å) with exposure time of 4 min at the Beamline of 10.3.2 at the Advanced Light Source. A Bruker APEX2 CCD detector was used, and the obtained XRD pattern was calibrated using α-Al_2O_3 powder. Powder X-ray diffraction (XRD) pattern of Eu^{2+} doped CsCl nanocrystals was measured on a Bruker AXS D8 Advance diffractometer with a Cu Kα source (X-ray wavelength of 1.54 Å). The transmission electron microscopy (TEM) images were taken on a Hitachi H7650 at an accelerating voltage of 120 kV. High-resolution TEM (HRTEM) images were taken with a FEI Tecnai TEM at an accelerating voltage of 200 kV. The energy-dispersive X-ray spectroscopy (EDS) elemental mapping images were recorded using an FEI Titan microscope operated at 80 kV. This instrument was equipped with an FEI Super-X Quad windowless detector that is based on silicon drift technology. Elemental quantification data was analyzed using the Bruker Esprit EDS analysis package, which has been calibrated against mineral standards for quantitative accuracy.

Absorption spectra were collected using a Shimudzu UV-2600 PC UV-VIS-IR scanning spectrophotometer equipped with a Shimadzu ISR-3100 integrating sphere. Solution Photoluminescent (PL) and Time-Resolved PL (TRPL) spectra were measured using a PicoQuant Fluotime 300, equipped with a PMA 175 detector and a LDH-P-C-405 diode laser with an excitation wavelength of 407.1 nm. Photoluminescent PL Excitation (PLE) were measured using a PicoQuant FluoTime 300 Fluorimeter. The sample was excited using a Xenon lamp and the emission at 435 nm was collected using a monochrometer

with a bandpass filter to block excitation scatter. For the nanocrystals embedded in PMMA, the thin film sample was excited by a continuous-wave solid state laser at 375 nm (Coherent OBIS 375LX) with a laser filter (bandpass, 375 nm/6 nm). Photoluminescence quantum yield (PLQY) was measured in a photoluminescence system coupled with an integration sphere. The excitation at 375 nm was focused onto the sample and then the spectra were taken by the grating-based spectrograph (Princeton Instrument, SP-2300i) with the acquisition time of 1s for each measurement.

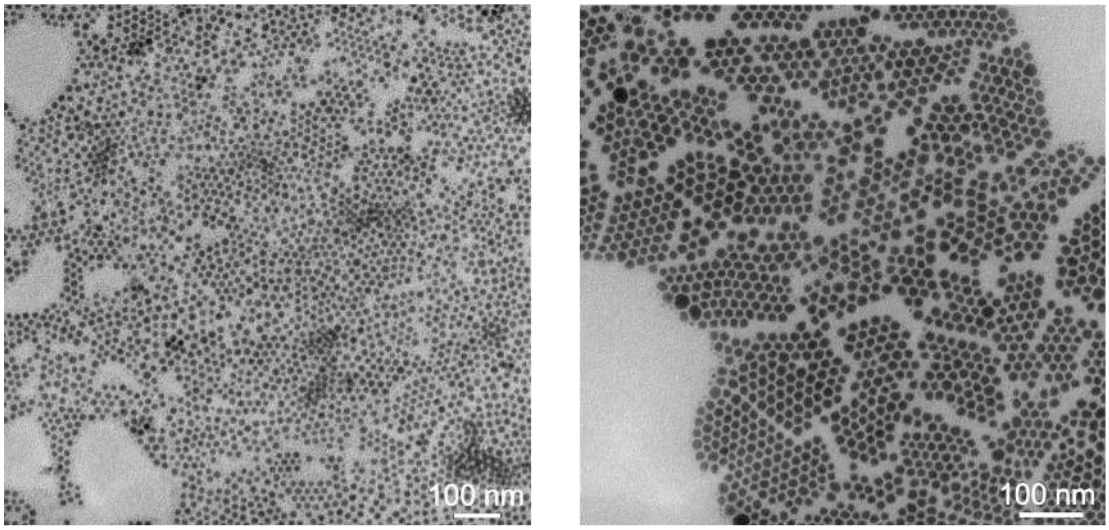

Figure S1 Representative low-magnification TEM images of $CsEuCl_3$ nanocrystals.

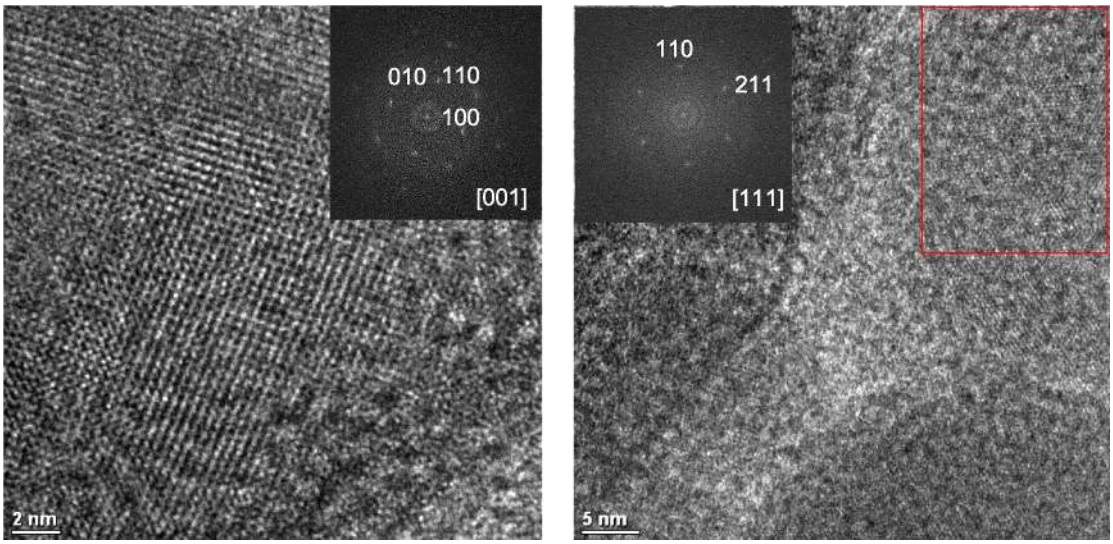

Figure S2 More HRTEM images and corresponding FFT of $CsEuCl_3$ nanocrystals.

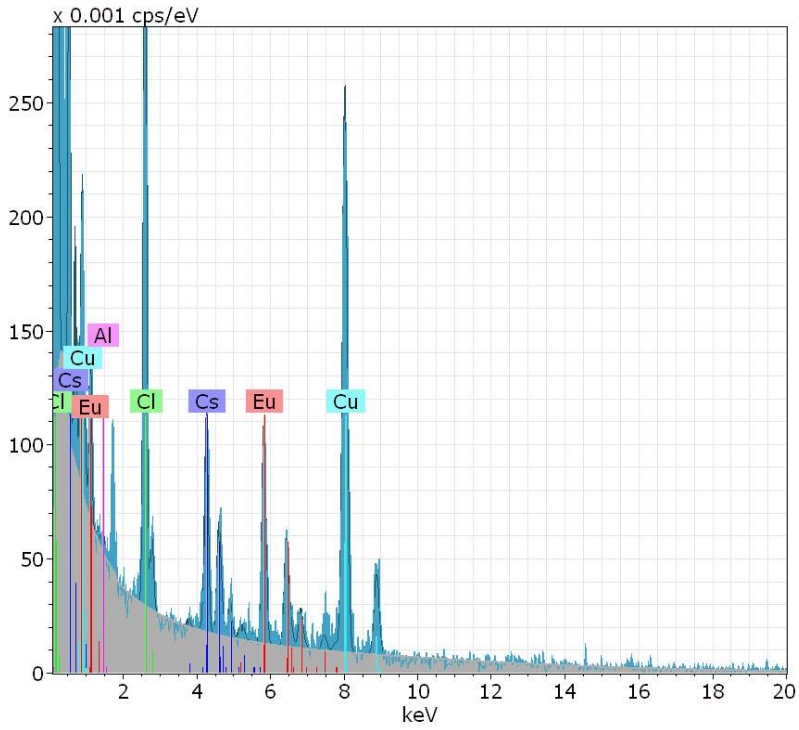

Figure S3 EDS spectrum of $CsEuCl_3$ nanocrystals.

Table S1 EDS measured atomic ratio of $CsEuCl_3$ nanocrystals.

Elements	Stoichiometric atomic %	Measured atomic %
Cs	20	18.4
Eu	20	20.2
Cl	60	61.4

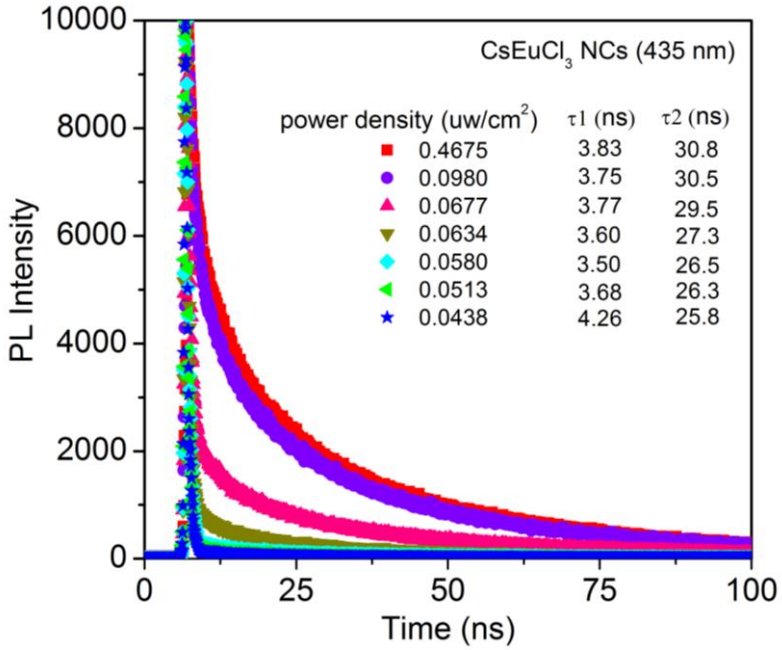

Figure S4 Power dependent time-resolved photoluminescence spectra measured at a wavelength of 435 nm for $CsEuCl_3$ nanocrystals.

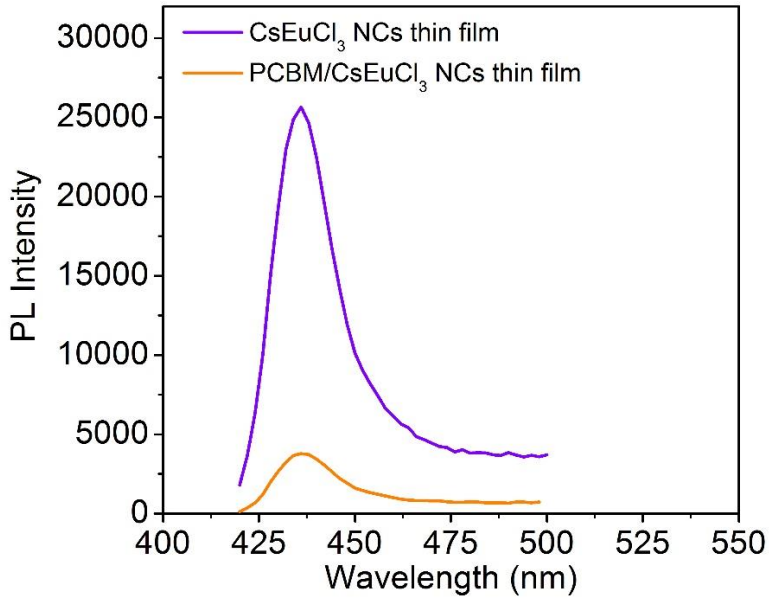

Figure S5 Photoluminescence spectra of $CsEuCl_3$ nanocrystals thin film, and phenyl-C_{61}-butyric acid methyl ester (PCBM) thin film on top of $CsEuCl_3$ nanocrystals thin film. These two samples were measured at the same power of laser.

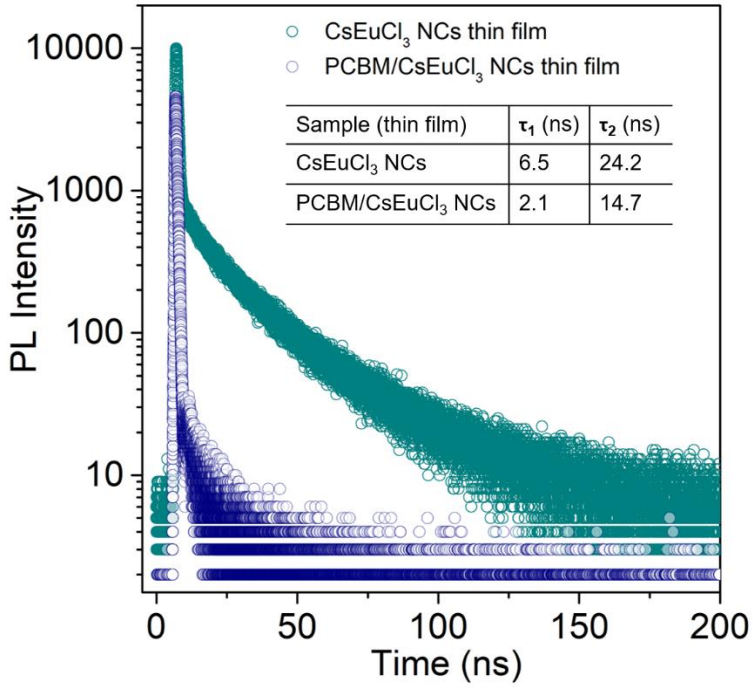

Figure S6 Time-resolved photoluminescence spectra measured at a wavelength of 435 nm for $CsEuCl_3$ nanocrystals thin film, and phenyl-C_{61}-butyric acid methyl ester (PCBM) thin film on top of $CsEuCl_3$ nanocrystals thin film.

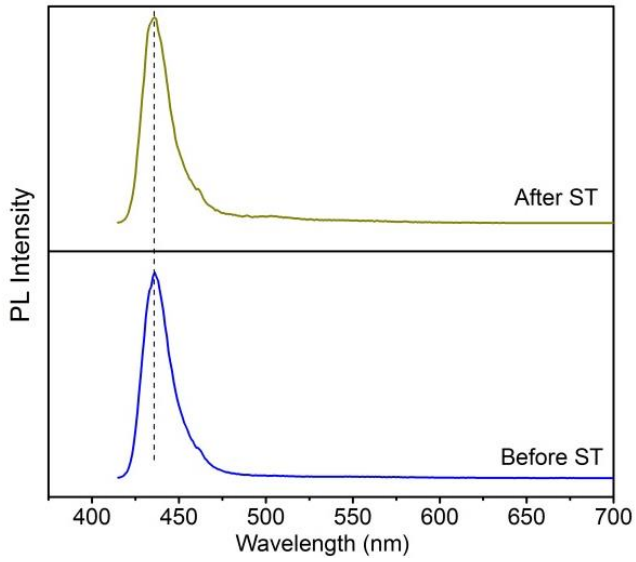

Figure S7 Photoluminescence spectra of $CsEuCl_3$ nanocrystals before and after surface treatment (ST) with 1-butyl-1-methylpyridinium chloride.

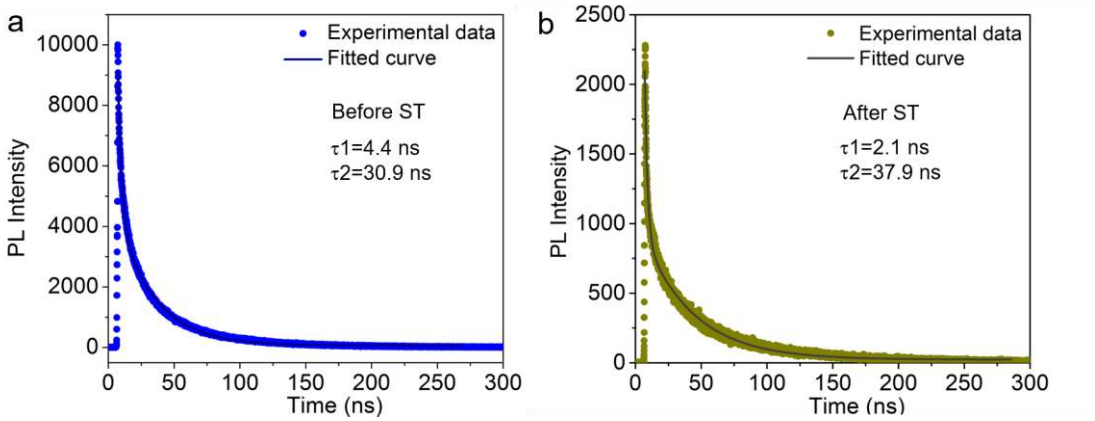

Figure S8 Time resolved photoluminescence spectra of $CsEuCl_3$ nanocrystals before and after surface treatment (ST) with 1-butyl-1-methylpyridinium chloride.

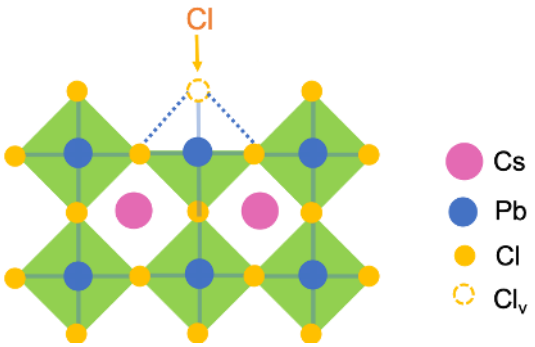

Figure S9 Schematic representation of mechanism of surface treatment with 1-butyl-1-methylpyridinium chloride. 1-butyl-1-methylpyridinium chloride acts as a chlorine source to substitute the chloride vacancy in the nanocrystal surface.

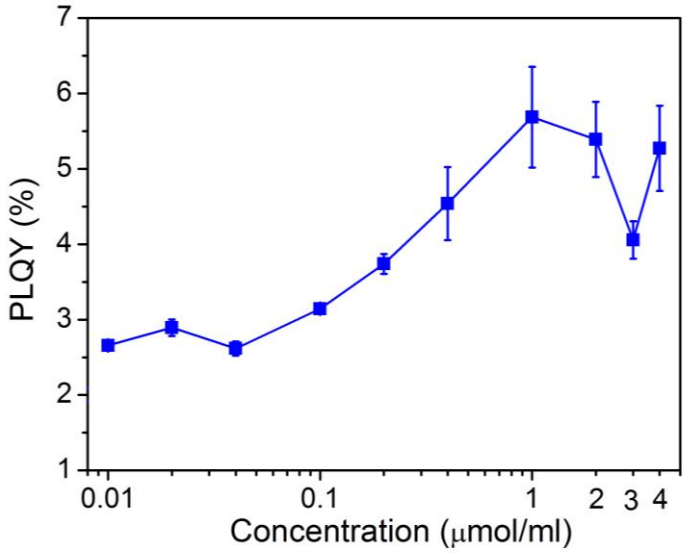

Figure S10 The photoluminescence quantum efficiency yield (PLQY) changes as the 1-butyl-1-methylpyridinium chloride concentration increases.

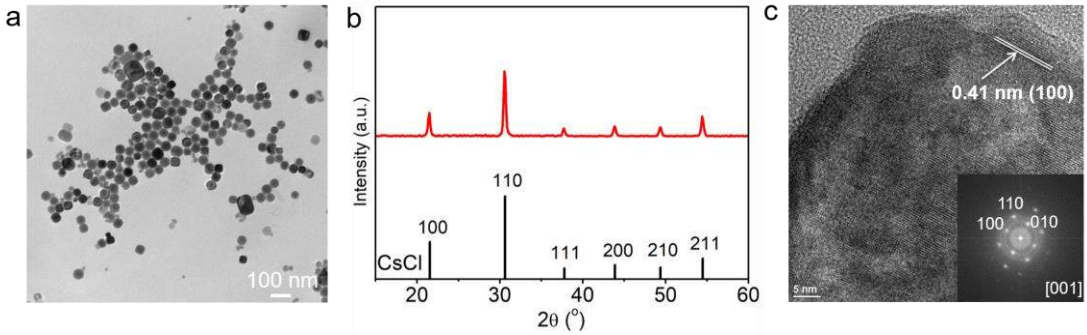

Figure S11 (a) Representative TEM image, (b) XRD pattern, (c) HRTEM and corresponding FFT (inset) of Eu^{2+} doped CsCl nanocrystals. X-ray wavelength λ = 1.54 Å.

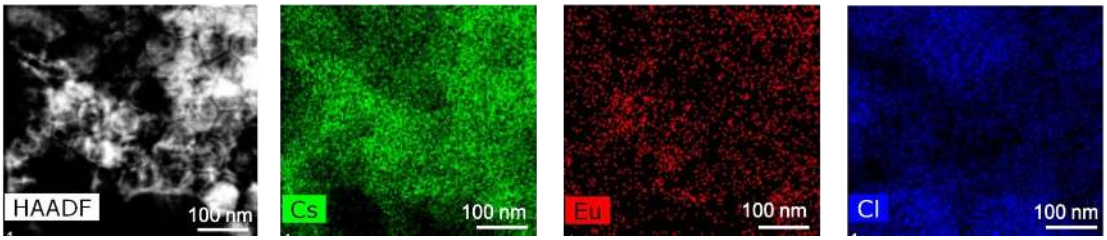

Figure S12 EDS mapping of Eu^{2+} doped CsCl nanocrystals.

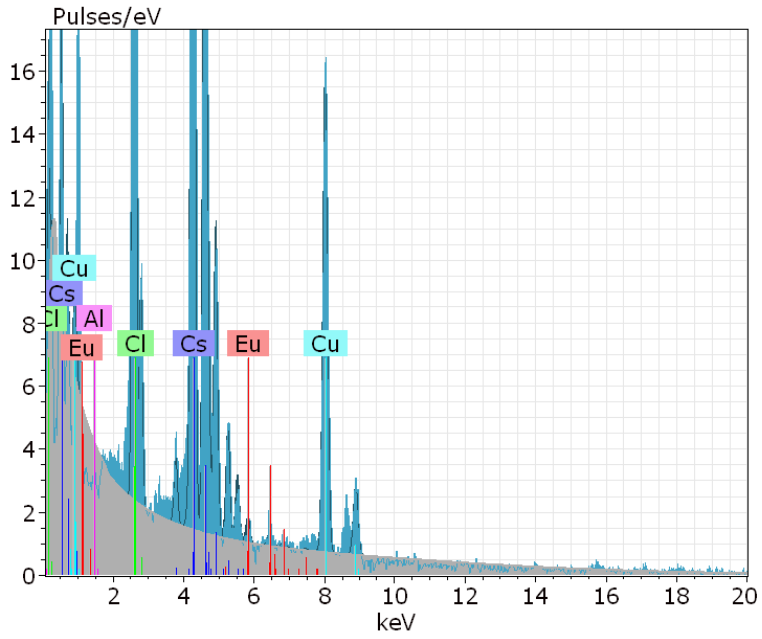

Figure S13 EDS spectrum of Eu^{2+} doped CsCl nanocrystals.

Table S2 EDS measured atomic ratio of Eu^{2+} doped CsCl nanocrystals.

Elements	Measured atomic %
Cs	41.0
Eu	1.3
Cl	57.7

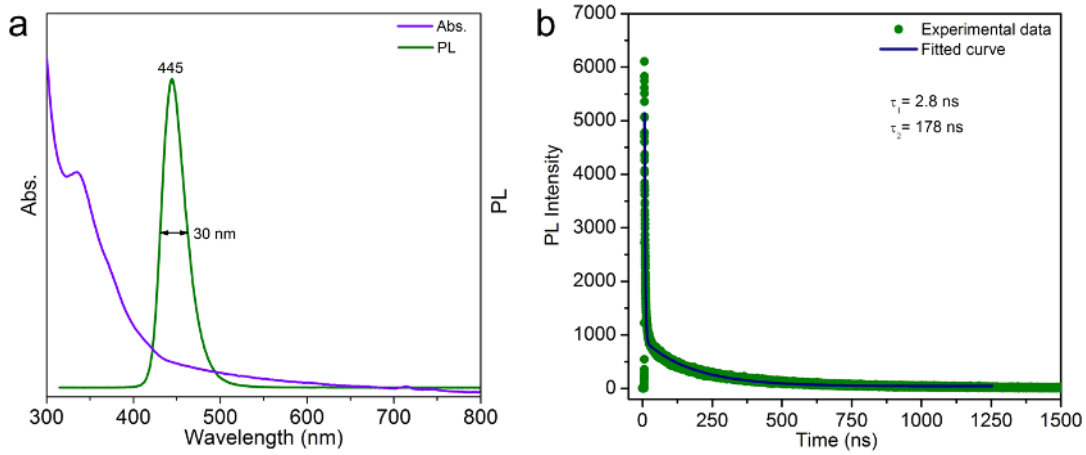

Figure S14 (a) Optical absorption and photoluminescence spectra of Eu^{2+} doped CsCl nanocrystals. (b) Time-resolved photoluminescence spectra measured at wavelength of 445 nm. The data was fitted using a bi-exponential decay function.

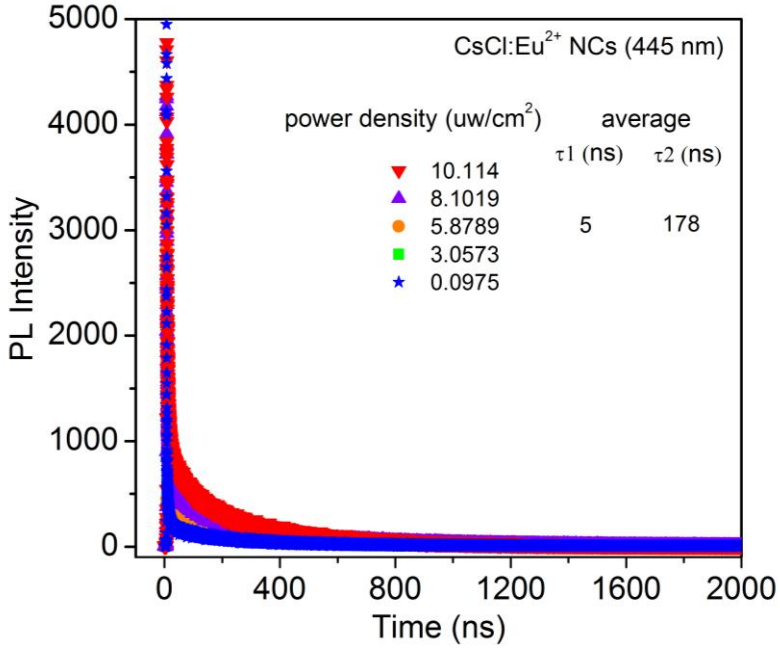

Figure S15 Power dependent time-resolved photoluminescence spectra measured at a wavelength of 445 nm for Eu^{2+} doped CsCl nanocrystals.

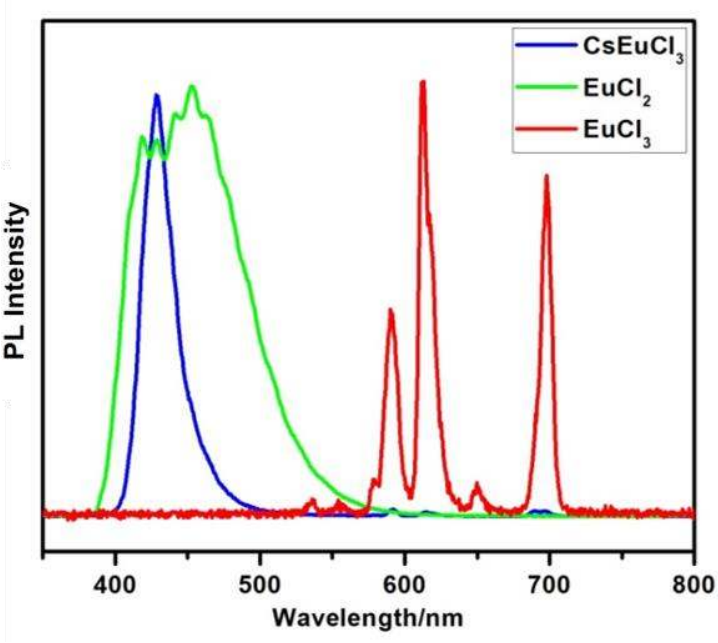

Figure S16 Photoluminescence spectra $CsEuCl_3$ single crystal, precursors of $EuCl_2$ and $EuCl_3$.

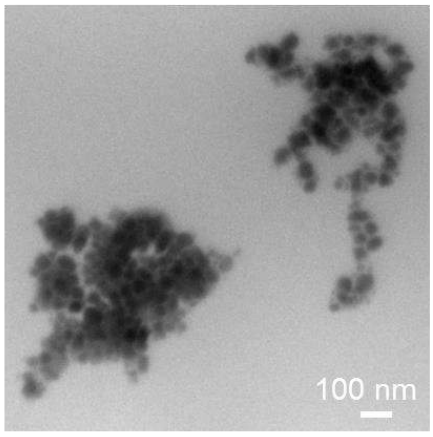

Figure S17 TEM image of the $CsEuCl_3$ nanocrystals embedded in PMMA.